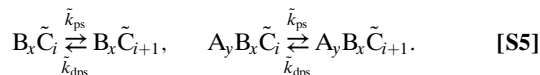
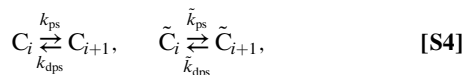
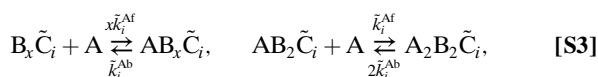
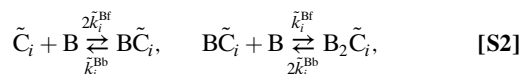
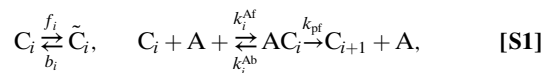


# Supporting Information

Zwicker et al. 10.1073/pnas.1007613107

## SI Text

**S1. The Models. S1.1. PPC-in vitro model: A PPC with constant protein copy numbers.** Fig. 1B of the main text shows a cartoon of the PPC-in vitro model. In this model of the protein phosphorylation cycle (PPC) the total concentration of each Kai protein is constant. The model is described by reactions 1–5 of the main text, which we repeat here:



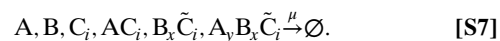
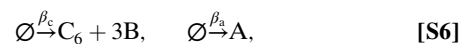
Here,  $C_i$  denotes a KaiC hexamer in the active conformational state, in which the number  $i$  of phosphorylated monomers tends to increase, and  $\tilde{C}_i$  denotes a KaiC hexamer in the inactive conformational state in which  $i$  tends to decrease; A denotes a KaiA dimer, and B denotes a KaiB dimer. The reactions  $C_i \rightleftharpoons \tilde{C}_i$  in **S1** model the conformational transitions between active and inactive KaiC; the second set of reactions in **S1** describe phosphorylation of active KaiC that is stimulated by KaiA; the reactions in **S2** model the binding of KaiB to inactive KaiC and those in **S3** model the sequestration of KaiA by inactive KaiC that is bound to KaiB; note that an inactive KaiC hexamer can bind up to two KaiA dimers; the reactions in **S4** and **S5** model spontaneous phosphorylation and dephosphorylation of active and inactive KaiC. For a more detailed discussion of the model, we refer to ref. 1.

We study this model, as well as the other stochastic models discussed below, using kinetic Monte Carlo simulations of the chemical master equation (2). In our simulations, we vary the reaction volume, but keep the concentrations of the Kai proteins constant at levels comparable to those used in the in vitro experiments (3, 4). Fig. S1A shows two time traces of the phosphorylation level  $p(t)$ , defined as the fraction of monomers that is phosphorylated, for two different volumes, whereas Fig. 2 of the main text shows the correlation number of cycles,  $n_{1/2}$ , as a function of the volume; for a discussion of how  $n_{1/2}$  is computed, see section S7.

**Comparing the robustness with in vivo measurements.** Fig. 2 of the main text shows that  $n_{1/2}$  increases with the volume. To compare our predictions with the experimental results obtained in vivo (5), we have to verify that the concentrations of the Kai proteins in

vitro/in silico are similar to those in vivo, because the behavior of the phosphorylation cycle depends on the concentrations of the Kai proteins (3, 4). The copy number of KaiC monomers in vivo has been measured (6) to be around 10,000, corresponding to roughly 1,000 KaiC hexamers, which, assuming that the bacterium is roughly 1 cubic micron, corresponds to a KaiC hexamer concentration of about 1  $\mu\text{M}$ , comparable to the KaiC hexamer concentration in vitro (3, 4). It thus seems meaningful to compare the predictions of Fig. 2 of the main text with experiment. Our model predicts that for a bacterial volume of 1 cubic micron, the phosphorylation cycle is highly robust, with  $n_{1/2} \approx 200$ , in agreement with what has been measured experimentally in vivo, which is  $n_{1/2} = 166 \pm 100$  days (5). However, the number of KaiA monomers in vivo has been measured to be on the order of 250–500 monomers (6), corresponding to 125–250 KaiA dimers. This means that in vivo the concentration ratio of KaiA dimers to KaiC hexamers is about 1:6, which is lower than the corresponding ratio in the test tube, which is 1:1 (3). In fact, for the in vivo concentration ratio of KaiA to KaiC, the in vitro system does not exhibit macroscopic phosphorylation oscillations (3, 4). It has therefore been suggested that in vivo the oscillations are confined to a small subcellular domain from which some KaiB and KaiC molecules are excluded (6), allowing the reactions to proceed at roughly the in vitro ratio; here, we adopt this hypothesis and assume that the Kai proteins are found in the physiologically relevant reaction volume in proportions comparable to those used in the in vitro experiments. If we take this volume to be a third of the total bacterial volume, i.e.,  $V \sim 0.3 \mu\text{m}^3$ —small enough that the measured number of KaiA molecules is more than adequate to give the in vitro KaiA dimer concentration of 0.58  $\mu\text{M}$  (3, 4)—then our model predicts that the phosphorylation cycle has a correlation time of roughly 75 days. This would still be consistent with the value measured experimentally (5), in contrast to the models proposed by Eguchi et al. (7) and Rust et al. (8) (see section S5). Our model thus predicts that the phosphorylation cycle is highly robust against the intrinsic noise arising from the stochastic nature of the phosphorylation reactions and the physical interactions between the Kai proteins.

**S1.2. PPC-in vivo model: A PPC with constant protein synthesis and degradation rates.** In the main text, we also discuss the performance of a model that includes not only a PPC, but also synthesis and degradation of the Kai proteins; we call this model the PPC-in vivo model. This model is described in reactions **S1–S5** plus the following reactions for the synthesis and degradation of the Kai proteins:



As explained in the main text, we assume that fresh KaiC is injected into the system as fully phosphorylated hexamers because phosphorylation of fresh KaiC proteins has been reported to be fast, i.e., occurring within 30 min (9). However, the precise choice for the phosphoform of fresh KaiC is not so important in this model; it does not affect the robustness of this model. Because the KaiB and KaiC proteins are both products of the *kaiBC* operon, we choose to model the production of both proteins as a single reaction. We note that while in the model with the transcription–translation cycle, discussed in section S1.4, the delay

in the synthesis reactions is critical, in the above model, where the Kai proteins are produced with rates that are constant in time, a delay would have no effect; the synthesis reactions are therefore modeled as simple, Poissonian birth reactions. Fig. S1B shows time traces for the phosphorylation level  $p(t)$  for three different degradation rates.

**51.3. Deterministic PPC-in vivo model.** To verify that the disappearance of oscillations as the degradation rate is increased is not a purely stochastic effect, we consider the model of S1–S7 in the deterministic limit of infinite volume and protein number. In this limit, the concentrations of the different proteins evolve according to deterministic rate equations. We make two further simplifying assumptions: First, we replace the two-step binding of KaiB to  $\tilde{C}_i$  with a trimolecular reaction that turns  $\tilde{C}_i$  directly into  $B_2\tilde{C}_i$ , and making a similar change for binding of KaiA to the inactive branch. Second, we assume that binding and unbinding reactions are fast enough that they are effectively in steady state and thus explicitly keep track only of the concentrations of the various KaiC species; the concentrations of free KaiA and KaiB can then be inferred from conservation laws. The dynamical equations are then essentially the same as those given in equations 44–47 of our previous publication (1), with the addition of a linear decay term with rate  $\mu$  for each species and of synthesis of  $C_6$  with rate  $\beta_c$ :

$$\frac{d[C_i]_T}{dt} = \sigma_{i-1}^{ps}[C_{i-1}]_T + \sigma_{i+1}^{dps}[C_{i+1}]_T - (\sigma_i^{ps} + \sigma_i^{dps})[C_i]_T - \sigma_i^{ff}[C_i]_T + \sigma_i^{fb}[\tilde{C}_i] + \beta_c \delta_{i,6} - \mu[C_i]_T, \quad [S8]$$

$$\frac{d[\tilde{C}_i]}{dt} = \tilde{k}_{ps}[\tilde{C}_{i-1}] + \tilde{k}_{dps}[\tilde{C}_{i+1}] - (\tilde{k}_{ps} + \tilde{k}_{dps})[\tilde{C}_i] + \sigma_i^{ff}[C_i]_T - \sigma_i^{fb}[\tilde{C}_i] - \tilde{\kappa}_i^{bf}([B])_T - 2\Sigma_i[B_2\tilde{C}_i]_T^2[\tilde{C}_i] + \frac{\tilde{\kappa}_i^{bb}\tilde{K}_i[B_2\tilde{C}_i]_T}{\tilde{K}_i + [A]^2} - \mu[\tilde{C}_i], \quad [S9]$$

$$\frac{d[B_2\tilde{C}_i]_T}{dt} = \tilde{k}_{ps}[B_2\tilde{C}_{i-1}]_T + \tilde{k}_{dps}[B_2\tilde{C}_{i+1}]_T - (\tilde{k}_{ps} + \tilde{k}_{dps})[B_2\tilde{C}_i]_T + \tilde{\kappa}_i^{bf}([B])_T - 2\Sigma_i[B_2\tilde{C}_i]_T^2[\tilde{C}_i] - \frac{\tilde{\kappa}_i^{bb}\tilde{K}_i[B_2\tilde{C}_i]_T}{\tilde{K}_i + [A]^2} - \mu[B_2\tilde{C}_i]_T, \quad [S10]$$

where the concentration of free KaiA,  $[A]$ , is given by

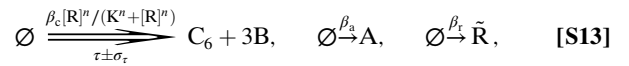
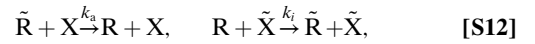
$$[A] + \sum_{i=0}^N \frac{[A][C_i]_T}{\tilde{K}_i + [A]} + 2 \sum_{i=0}^N \frac{[A]^2[B_2\tilde{C}_i]_T}{\tilde{K}_i^2 + [A]^2} - [A]_T = 0. \quad [S11]$$

Here  $[C_i]_T$  is the total concentration of KaiC hexamers with  $i$  phosphorylated monomers in the active state, whether or not complexed with KaiA, i.e.,  $[C_i]_T = [C_i] + [AC_i]$ ;  $[B_2\tilde{C}_i]_T$  is defined similarly. The effective rate constants appearing in these equations depend on the concentration  $[A]$  of free KaiA and are defined in terms of the more microscopic rate constants as follows: The effective (de)phosphorylation rates on the active branch are  $\sigma_i^{ps} = (k_{ps}K_i + k_{pf}[A])/(K_i + [A])$  and  $\sigma_i^{dps} = K_i k_{dps}/(K_i + [A])$ . The effective flipping rates are given by  $\sigma_i^{ff} = f_i K_i/(K_i + [A])$  and  $\sigma_i^{fb} = b_i$ , where  $f_i$  and  $b_i$  are the forward and backward flipping rates. The parameters  $\tilde{\kappa}_i^{bf}$  and  $\tilde{\kappa}_i^{bb}$  differ from  $\tilde{k}_i^{bf}$  and  $\tilde{k}_i^{bb}$ , respectively, in that the  $\kappa$ 's are rate constants for trimolecular reactions, which are broken down into two successive bimolecular reactions in the stochastic simulations. The dissociation constants  $K_i$  satisfy  $K_i = k_i^{Ab}/k_i^{Af}$ ; the  $\tilde{K}_i$  could be defined similarly in terms

of forward and backward rates for KaiA binding to the inactive branch, but (just as with  $\tilde{\kappa}_i^{bf}$  and  $\tilde{\kappa}_i^{bb}$ ) these rates would differ from those used in the stochastic simulations, so we choose instead to quote the dissociation constants directly. Following ref. 1, we choose values for the new parameters associated with trimolecular interactions such that time dependence of  $p(t)$  matches the average behavior of the stochastic model.

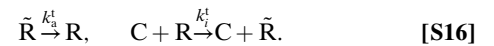
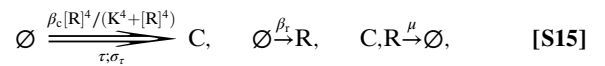
To determine where oscillations disappear as  $\mu$  is increased, we analyzed these equations using the XPPAUT implementation of the AUTO continuation package (10). We found that, for the parameter values given in Table S1, the system undergoes a supercritical Hopf bifurcation at  $\mu = 0.0621 \text{ h}^{-1}$ , as noted in the main text.

**51.4. PPC-TTC model: The PPC and TTC combined.** The PPC-TTC model of the main text consists of a PPC, a transcription–translation cycle (TTC), and a pathway that couples these two cycles. This model is described by the reactions of S1–S5 for the PPC, together with the following reactions for the TTC and the coupling between them:



Here,  $R$  and  $\tilde{R}$  denote the RpaA protein in its active and its inactive form, respectively, whereas  $n$  is the Hill coefficient of gene repression; its baseline value is  $n = 4$ , but in section S4.3 we study the effect of varying  $n$ . The  $X$  and  $\tilde{X}$  in S12 denote any of the phosphoforms of KaiC that mediate the activation and repression of RpaA, respectively; in section S4.1, we discuss the dependence of the results on precisely which phosphoforms are chosen to activate and repress RpaA, respectively. The double arrow indicates a reaction with a Gaussian distributed delay with mean  $\tau$  and variance  $\sigma_\tau$ . We thus assume that *kaiBC* expression is activated by RpaA, where the activity of RpaA is modulated by the PPC. In contrast, the expression of KaiA, KaiB, and RpaA is assumed to occur constitutively. Fig. S1C shows time traces for the phosphorylation level  $p(t)$  and total KaiC concentration  $[C]_T(t)$  for  $V = 1 \mu\text{m}^3$  and  $\mu = 0.03 \text{ h}^{-1}$  (solid lines) and  $\mu = 0.1 \text{ h}^{-1}$  (dotted lines), respectively.

**51.5. TTC-only model.** The TTC-only model is given by the following reactions:



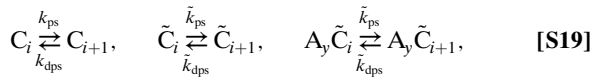
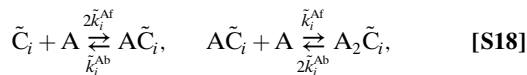
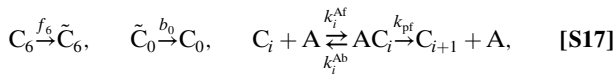
In the simulations, we adjust the delay  $\tau$  and the synthesis rate  $\beta_c$  for each choice of the degradation rate  $\mu$  such that the oscillation period is 24 h and the average KaiC concentration is comparable to that of the other models considered so far. Fig. S1D shows time traces for the concentrations of KaiC and active RpaA, respectively. In section S2 we discuss the simplest possible TTC model, namely one in which KaiC directly represses its own synthesis; this gave very similar results.

**51.6. Parameters.** Table S1 gives the values of the parameters used in the stochastic simulations based on the kinetic Monte Carlo algorithm developed by Gillespie (2). Unless otherwise noted,

we choose the total concentrations of the Kai proteins to match common conditions for the *in vitro* reaction system (3, 4):  $[A]_T = 0.58 \mu\text{M}$ ,  $[B]_T = 1.75 \mu\text{M}$ , and  $[C]_T = 0.58 \mu\text{M}$ .

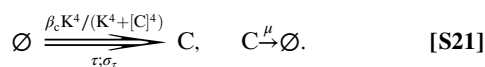
**S2. A Simplified Description Provides Insight into the PPC-TTC Model's Robustness.** To elucidate why a clock built upon a TTC and a PPC is robust across a range of protein turnover rates, we study minimal versions of the models discussed above. We also introduce two new models, the *PMS-TTC* model and the *UPPC-TTC* model, that represent intermediate cases between the extremes of the coupled *PPC-TTC* model on the one hand and the separate *PPC-in vivo* and *TTC-only* models on the other. Cartoons of these new models are shown in Fig. S2 A–D. Below, we first briefly describe the different models and then use them to explain why a PPC enhances the robustness of a TTC, and vice versa. Throughout this section, we refer to the more realistic models introduced in the main text, and discussed in the preceding section, as *full* models, while the simplified versions considered in this section are called *minimal* models. The parameters of the minimal models are shown in Table S1.

**Minimal PPC-in vivo model.** In the minimal *PPC-in vivo* model, the binding of KaiB to KaiC has been integrated out and intermediate conformational transitions between active and inactive KaiC are disallowed. The model is described by the following reactions:



These equations give a generic description of a protein modification cycle that is synchronized via the mechanism of differential affinity (1), in which KaiA sequestration synchronizes the phosphorylation cycles of different KaiC hexamers. The solid red line of Fig. S2E shows the correlation number of cycles,  $n_{1/2}$ , as a function of the degradation rate  $\mu$  for  $V = 1 \mu\text{m}^3$  for this minimal *PPC-in vivo* model; when  $\mu$  is varied, the protein synthesis rates are adjusted such that the average protein concentrations are unchanged. The minimal model's behavior is not only qualitatively, but also quantitatively very similar to that of the full *PPC-in vivo* model (Fig. 5 of main text); in particular, the PPC alone is stable only at low protein degradation rates.

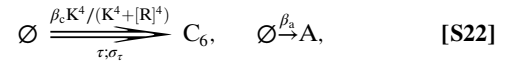
**Minimal TTC-only model.** The simplest and most generic TTC model is one in which KaiC directly represses its own synthesis (with a delay, indicated by a double arrow as in the main text):



It can be seen that in comparison to the *TTC-only* model of the main text, here RpaA has been integrated out. The green line of Fig. S2E shows  $n_{1/2}$  as a function of  $\mu$  for  $V = 1 \mu\text{m}^3$ ; when  $\mu$  is varied, both the protein synthesis rate  $\beta_c$  and the delay in protein synthesis  $\tau$  are adjusted such that the average KaiC concentration

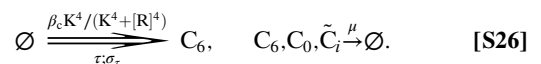
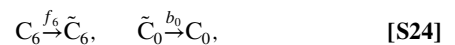
and the oscillation period remain constant. The minimal model behaves very similarly to the full *TTC-only* model discussed in the main text (see Fig. 5), showing robust oscillations only for high protein turnover rates.

**Minimal PPC-TTC model.** The PPC of the minimal *PPC-TTC* model is given by the minimal PPC described above (S17–S20). In the full *PPC-TTC* model, the active KaiC phosphoforms activate RpaA and thereby stimulate KaiC synthesis, whereas the inactive KaiC phosphoforms deactivate RpaA and thereby repress KaiC synthesis. In the minimal *PPC-TTC* model, we have integrated out RpaA. Moreover, we assume that only the inactive KaiC phosphoforms regulate, i.e., repress, KaiC synthesis. This yields the following synthesis and decay reactions:



Here,  $[R] = \sum_{i=0}^6 (\tilde{C}_i + [A\tilde{C}_i] + [A_2\tilde{C}_i])$  is the total concentration of all the KaiC phosphoforms that are in the inactive state. The blue line of Fig. S2E shows the correlation number of cycles  $n_{1/2}$  as a function of the degradation rate  $\mu$  for  $V = 1 \mu\text{m}^3$  for this model. As  $\mu$  is varied, the protein synthesis rates are adjusted to keep the average protein concentrations constant, but it turns out not to be necessary to change the delay  $\tau$  in protein synthesis, because the period of the clock is dictated primarily by the PPC (see section S6 for a more detailed discussion). As expected, the behavior of the minimal *PPC-TTC* model is similar to that of the full *PPC-TTC* model discussed in the main text; the clock is robust not only in the limiting regimes of low and high protein turnover rates, but also in the biologically relevant crossover regime.

**Minimal PMS-TTC model.** This model is meant to capture one possible effect on the TTC of coupling it to the PPC: Rather than disappearing only through first-order degradation at a rate  $\mu$ , as they do in the *TTC-only* model, the KaiC forms that repress transcription can also, when a PPC is present, be eliminated by their advance through KaiC's phosphorylation cycle, which must eventually turn repressing hexamers  $\tilde{C}_i$  on the inactive branch into active hexamers  $C_i$  that do not affect transcription. Moreover, because progress through the phosphorylation cycle involves a sequence of first-order steps, the distribution of times for repressors to disappear via this new route will be narrower than the distribution of degradation times, which should in turn increase the clock's robustness. To elucidate these effects, the *PMS-TTC* model combines a TTC with a protein modification sequence (PMS): The proteins do not undergo a full cycle of protein modification steps, as in the original PPC, but a half cycle, during which they progress through a *sequence* of repressive KaiC phosphoforms before being converted into the  $C_0$  form that cannot regulate transcription. The model is described by the following reactions:

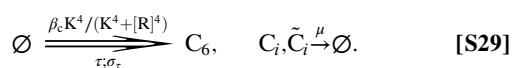
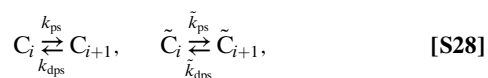


Here,  $[R] = \sum_{i=0}^6 [\tilde{C}_i]$  is the total concentration of inactive KaiC, which represses *kaiC*. Note that, in order to maintain as close a correspondence as possible with the *PPC-TTC* model, KaiC is



produced in its fully phosphorylated, but active, state,  $C_6$ . Because the flip rate from  $C_6$  to  $\tilde{C}_6$  is much faster than the dephosphorylation rate, however, this has essentially no effect on the dynamics. In contrast, the reaction from  $C_0 \rightarrow C_0$  is critical: Omitting it would yield a model that behaves *exactly* as the TTC-only model—dephosphorylation would merely change the phosphorylation *label* of KaiC, but not the dynamics of *kaiC* repression. In order for protein modification to have an effect on the temporal regulation of *kaiC* repression, it is essential that KaiC can leave the modification states in which it represses *kaiC* via a reaction other than degradation. It should also be noted that, in order to compare the *PMS-TTC* model with the *PPC-TTC* model, the dephosphorylation reactions have the same rates as in the *PPC-TTC* model. As for the *TTC-only* model, when  $\mu$  is varied, both the protein synthesis rate  $\beta_c$  and the delay in protein synthesis  $\tau$  are adjusted so that the average KaiC concentration and the oscillation period remain constant. When  $\mu \ll k_{dps}$ , the gene-repressing phosphoforms turn into the nonrepressing  $C_0$  state via protein dephosphorylation before they are degraded, and one might thus think that the model's behavior is completely independent of  $\mu$  in this limit. However,  $C_0$  is part of the total KaiC concentration, which we fix by adjusting  $\beta_c$  for each  $\mu$ ; and because  $\beta_c$  does affect the behavior of the system as described below,  $\mu$  remains an important control variable, even when  $\mu \ll k_{dps}$ . The magenta line of Fig. S2E shows the correlation number of cycles  $n_{1/2}$  as a function of the protein degradation rate  $\mu$  for  $V = 1 \mu\text{m}^3$  for the *PPC-TTC* model. It is more robust than the *TTC-only* model, with sustained oscillations for lower values of the protein degradation rate. Nonetheless, the oscillations still cease to exist for small enough  $\mu$ .

**Minimal UPPC-TTC model.** This model probes the ability of the TTC to synchronize the PPC. To this end, it combines a TTC with an unsynchronized protein phosphorylation cycle (UPPC). Each protein undergoes a full cycle of protein modification steps as in the original PPC, but the cycles of the individual proteins (KaiC hexamers) are not synchronized as in the original PPC—KaiA, and thus the differential-affinity synchronization mechanism, has been removed. The model is defined by the reactions



Here,  $[R] = \sum_{i=0}^6 [\tilde{C}_i]$  is, as in the other minimal models, the total concentration of the KaiC phosphoforms that repress *kaiC* expression. The light blue line of Fig. S2E shows the robustness of this model,  $n_{1/2}$ , as a function of the protein turnover rate  $\mu$  for  $V = 1 \mu\text{m}^3$ ; when  $\mu$  is varied, the protein synthesis rates are adjusted to keep the average protein concentrations constant. (As with the *PPC-TTC* model, the period is largely determined by the phosphorylation cycle.) Its behavior in the limit of high protein degradation rate is similar to that of the *PMS-TTC* model, but the oscillations disappear more gradually as  $\mu$  is decreased, and even in the limit of low protein turnover rate, the system shows damped oscillations, leading to a  $n_{1/2}$  value of about 1–2 days.

**Toward a mechanism for robustness.** In section E of the main text, we argued that the *PPC-TTC* model is easily understood in the

limits of low and high degradation rates: At low degradation rates, a TTC by itself must fail, because it can generate only large amplitude oscillations if proteins are synthesized and destroyed on times scales faster than the oscillation period; one thus expects that the *PPC-TTC* clock is driven primarily by the PPC for small  $\mu$ . On the other hand, at high degradation rates, most KaiC proteins are destroyed before they can complete a full phosphorylation cycle, reducing the importance of the PPC. The TTC should thus be dominant when  $\mu$  is large. These expectations are borne out by the simulation results of Fig. S3. For small  $\mu$  (Fig. S3A), the total KaiC concentration is nearly constant in time, and oscillations in the concentration of KaiC phosphoforms that repress *kaiC* expression ( $[R]$ ) are driven almost entirely by the protein modification cycle of the PPC. For large  $\mu$  (Fig. S3B), in contrast,  $[R]$  tracks the total KaiC concentration almost perfectly, indicating that the oscillations arise primarily from periodic protein synthesis and degradation.

Although these limiting cases go a long way toward unraveling the behavior of the *PPC-TTC* model, they do not entirely explain the crossover regime when  $1/\mu$  is of order of the clock period and the combined *PPC-TTC* performs far better than the TTC or PPC alone. The *PMS-TTC* and *UPPC-TTC* models allow us to move away from the limiting cases and to examine how a PPC can *enhance* a TTC, and vice versa, in this crossover regime.

To explain why a PMS can enhance the stability of a TTC, we show in Fig. S3C time traces of the concentrations of the individual KaiC phosphoforms that repress *kaiC* in the *PMS-TTC* model, as well as their sum  $[R]$ ; for comparison, we also show a time trace of the KaiC concentration  $[C]$  in the *TTC-only* model. In the *TTC-only* model, the concentration of KaiC varies slowly and unreliably. In contrast, in the *TTC-PMS* model, the total repressor concentration  $[R]$  switches rapidly and strongly between a value that is well below the repression threshold and one that is well above it; this occurs because the concentrations of the individual KaiC phosphoforms rise and fall sharply as a result of the sequence of protein modification steps. These strong oscillations are beneficial because they minimize the effect of fluctuations in the repressor concentration on the timing of gene repression. To demonstrate this more clearly, we analytically compute for the *TTC-only* and the *PMS-TTC* models the distribution of times it takes to cross the gene repression threshold  $[R] = K$ , assuming that initially  $N$  molecules are present in the system that then decay either via protein degradation only, as in the *TTC-only* model, or via a combination of protein degradation and protein modification, as in the *PMS-TTC* model (see *Appendix* for details).

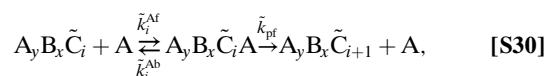
Fig. S3D shows the distribution of crossing times for both the *TTC-only* model and the *PMS-TTC* model, and for different values of the protein degradation rate  $\mu$ . It is seen that the crossing-time distribution of the *PMS-TTC* model is narrower than that of the *TTC-only* model, especially when the protein degradation rate is lower than the protein modification rate. Although in the *TTC-only* model gene repression is relieved only via protein degradation, involving a single Poisson process, in the *PMS-TTC* model gene repression can also be relieved via protein modification, which involves a sequence of Poissonian steps. The sequence of Poissonian steps leads to a narrower waiting-time distribution for crossing the repression threshold, and this explains why a protein modification sequence, which is a key characteristic of the PPC, can enhance the robustness of a TTC.

Although the protein modification sequence makes the *PMS-TTC* model more robust than the *TTC-only* model (Fig. S2E), the *PMS-TTC* model nonetheless is subject to the same fundamental bounds on its amplitude as a function of  $\mu$ , and it therefore does fail for protein degradation rates lower than about  $0.05 \text{ h}^{-1}$ . If we examine the simulation results in this regime in more detail, we can see that the immediate cause of the failure is an accumulation of molecules in the  $C_0$  state, leading the concentrations of KaiC phosphoforms that repress gene expression to drop below the re-

pression threshold permanently. The *UPPC-TTC* model differs from the *PMS-TTC* model in that it does not permit proteins to accumulate in one state, but instead includes an entire *cycle* through which molecules can be recycled to the  $\tilde{C}_6$  state. With such a cycle, coherent oscillations are in principle possible down to  $\mu = 0$ ; all that is required is a mechanism to synchronize the cycles of the different KaiC hexamers. In the models in which only a PPC is present, this synchronization is of course accomplished by the differential-affinity mechanism, but a moment's reflection reveals that the TTC must also have a synchronizing effect: When, once each oscillation period, a burst of proteins is produced in the  $C_6$  state, the distribution of phosphoforms not only shifts toward  $C_6$ , it also becomes narrower. Or, to phrase the argument slightly differently, while all KaiC hexamers are removed from the system at a rate that does not depend on the modification state, meaning that the protein removal process has no effect on the breadth of the phosphoform distribution, they are replaced by a synchronized group of proteins all in the same phosphorylation state, which means that the synthesis process does tend to narrow the distribution. This necessarily acts to synchronize the oscillation as a whole. With the *UPPC-TTC* model, in which this is the only synchronizing influence present, we can examine quantitatively how strong this effect is. To this end, we need to examine the stability of the *UPPC-TTC* in the regime  $0.02 < \mu < 0.05 \text{ h}^{-1}$ . In this regime, the *UPPC-TTC* model is much more stable than the *TTC-only* and the *PMS-TTC* models, showing that the PPC is the principal driver in this regime. Moreover, the stability of the *UPPC-TTC* model in this regime is higher than that in the limiting regime of low growth rate. This difference is due to the synchronizing effect of the TTC on the PPC. This idea is supported by the fact that the  $n_{1/2}$  values for the *UPPC-TTC* model and the *PPC-TTC* model begin to increase at almost the same degradation rate  $\mu$ . Taken together, these observations strongly suggest that the increased robustness of the *PPC-TTC* model in the crossover regime can be attributed in large measure to the additional synchronizing effect of the TTC.

In summary, our analysis suggests that at low protein turnover rates, where  $n_{1/2}^{PPC-TTC} \approx n_{1/2}^{PPC} \gg n_{1/2}^{TTC}$ , the PPC is the principal driver of the circadian clock; at somewhat higher  $\mu$ , where  $n_{1/2}^{PPC-TTC} > n_{1/2}^{PPC} \gg n_{1/2}^{TTC}$ , the PPC still drives the clock, but it needs help from the TTC to create macroscopic oscillations out of the phosphorylation cycles of the individual hexamers; at even higher values of  $\mu$ , where  $n_{1/2}^{PPC-TTC} > n_{1/2}^{TTC} \gg n_{1/2}^{PPC}$ , the TTC is the principal pacemaker, but its stability is enhanced by the protein modification sequence of the PPC; and at the highest turnover rates, where  $n_{1/2}^{PPC-TTC} \approx n_{1/2}^{TTC} \gg n_{1/2}^{PPC}$ , the TTC is the sole driver of the clock.

**S3. PPC-TTC Model: Rhythms of *kaiBC* Expression when *kaiA* Is Overexpressed.** Kitayama et al. have shown that *kaiBC* expression oscillates with a circadian period in the presence of an excess of KaiA, although it is not clear whether these oscillations are sustained or damped (17). Our *PPC-TTC* model of the main text, which is described by **S1–S5** and **S12–S14** above, generates oscillations in *kaiBC* expression with a period of 24 h when *kaiA* is overexpressed threefold, as shown in Fig. S4A. This figure shows that the phosphorylation level also exhibits weak oscillations, which are not seen experimentally; this is due to the fact that our PPC model neglects phosphorylation of inactive KaiC, which is known to occur at high KaiA concentrations (8). To rectify this, we have extended our model to include KaiA-stimulated phosphorylation of inactive KaiC, using the same reactions as those used for active KaiC; specifically, we add to the reactions of **S1–S5** and **S12–S14** the following reactions:



for each phosphorylation level  $i$ ; the rate constants equal those of the corresponding reactions of active KaiC, except that the KaiA-KaiC association rate is reduced by a factor of 100. All other rate constants are as in Table S1. We also include autoactivation of RpaA via



with  $k_a^m = 25 \text{ h}^{-1}$ . Autoactivation of RpaA becomes necessary because the concentrations of the KaiC phosphoforms that activate RpaA become very low when KaiA is in excess. (The freshly injected KaiC hexamers do not make it to the bottom of the phosphorylation cycle because of the excess KaiA.) This model not only matches the in vitro observation that when an excess of KaiA is added during the dephosphorylation phase, the phosphorylation level of KaiC rises immediately (8), but also reproduces the in vivo oscillations of the total amount of KaiC when KaiA is overexpressed (17), as shown in Fig. S4B.

**S4. Robustness of the PPC-TTC Model to Parameter Variations.** In this section, we discuss how robust our *PPC-TTC* model is to variations in a number of parameters. In the next subsection we show that the results are insensitive to details of the pathway that couples the PPC with the TTC. In subsection S4.2 we show that bursts in gene expression hardly reduce the stability of the clock. In the next two subsections we show that the stability of the clock is highly insensitive to the value of the Hill coefficient of gene repression as long as it is larger than one, and quite insensitive to the variance in the delay of protein synthesis. In essence, combining a PPC with a TTC enhances the robustness of the clock to variations in the parameters of the TTC, such as the magnitude of bursts in gene expression, the Hill coefficient, and the width of the delay distribution. Finally, in subsection S4.5 we study a model in which cell growth, cell division, and binomial partitioning of proteins upon cell division are modeled explicitly and show that, due to the stabilizing effect of the PPC, its behavior is similar to the model of the main text. In the next section, section S5, we discuss a different *PPC-TTC* model, namely one that is based upon the model of the PPC developed by Rust et al. (8).

**S4.1. Results are independent of details of the output pathway.** In this section, we show that the precise choice of the KaiC phosphoforms that activate and repress RpaA is not critically important for the existence of oscillations. Table S2 shows the different models that we have considered, and Fig. S5 A–C shows their time traces. It is seen that the time traces are very similar to those of the *PPC-TTC* model of the main text, which is model a in Table S2. The most significant difference can be observed for the time trace of RpaA in models d and e. In these models, not only  $C_x A$  activates RpaA, but also  $C_x$ , thus KaiC that is not bound to KaiA. The concentration of  $C_x A$  reaches zero during the dephosphorylation phase, and, as a result, the concentration of RpaA becomes zero during this phase in models a–c. However, the concentration of  $C_x$  does not reach zero during the dephosphorylation phase, and consequently, there is some residual activation of RpaA during this phase in models d and e. Nevertheless, RpaA activation during the dephosphorylation phase in these models does not manifest itself in the time traces of KaiC, because the concentration of active RpaA is still below the threshold for *kaiBC* expression. The oscillations of the phosphorylation level and total KaiC concentration are thus fairly similar in all models, although models d and e are less robust.

**S4.2. The effect of bursts.** In the *PPC-TTC* model of the main text, described in section S1 of this *SI Text*, we have concatenated transcription and translation into one gene-expression step. Moreover, we have ignored promoter-state fluctuations. Allowing

for the explicit formation and translation of mRNA (11), as well as for slow promoter-state fluctuations (12, 13), could lead to bursts in protein synthesis, which are expected to lower the robustness of the TTC. This could potentially lower the stability of the clock. To address this, we have performed simulations of a model in which KaiB and KaiC are produced in bursts. We assume that 5 KaiC hexamers and 15 KaiB dimers are formed in each gene-expression reaction (rather than the 1 and 3 of **S13**); this corresponds to typical burst sizes observed experimentally (11) in *Escherichia coli*. Formula **S13** is thus replaced by

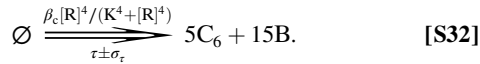


Fig. S5D shows the resulting phase diagram. It is similar to Fig. 4 of the main text, which shows the results of the *PPC-TTC* model without bursts in gene expression. The robustness of the model with bursts is lower, but not very much so:  $n_{1/2} = 150$  for the model with bursts versus  $n_{1/2} = 195$  for the model without bursts shown in the main text ( $\mu = 0.03 \text{ h}^{-1}$  and  $V = 1 \mu\text{m}^3$  in both cases). We believe that this relatively small reduction in the clock's stability is due to the stabilizing effect of the PPC.

**S4.3. Robustness to varying the Hill coefficient.** Fig. S5E shows for the full *PPC-TTC* model the correlation number of cycles,  $n_{1/2}$ , as a function of the degradation rate  $\mu$  for  $V = 1 \mu\text{m}^3$ , for four different values of the Hill coefficient of gene repression (see 7 of the main text and **S13**). It is seen that the stability of the clock is highly insensitive to the value of the Hill coefficient, except when the degradation rate is high: For  $\mu > 0.1 \text{ h}^{-1}$ , the oscillator becomes unstable when the Hill coefficient drops from 2 to 1. For lower values of  $\mu$  the PPC plays an important role in driving and stabilizing the clock; in fact, for  $\mu < 0.02 \text{ h}^{-1}$  the PPC is the sole driver, which means that in this regime the clock is not sensitive at all to variations in the parameters of the TTC (as long as the average concentrations and copy numbers remain constant). For  $\mu > 0.1 \text{ h}^{-1}$ , however, the TTC becomes the principal driver of the clock, which means that now the system does become sensitive to variations in the parameters of the TTC. It is known that oscillators built on only negative transcriptional feedback require a Hill coefficient that is larger than one to become stable (14). Our results are in line with these observations.

**S4.4. Robustness to the variance in the delay of protein synthesis.** Fig. S5F shows for the full *PPC-TTC* model the correlation number of cycles  $n_{1/2}$  as a function of the degradation rate  $\mu$  and the width of the distribution of the delay in protein synthesis,  $\sigma_r$  (see **S13**). It is seen that because of the stabilizing effect of the PPC the clock is essentially insensitive to variations in  $\sigma_r$ . Only for  $\mu > 0.1 \text{ h}^{-1}$ , when the TTC becomes the principal pacemaker of the clock, does  $n_{1/2}$  decrease when  $\sigma_r$  becomes larger than 3 h.

**S4.5. PPC-TTC model with volume growth and binomial partitioning.** Living cells constantly grow and divide, and proteins thus have to be synthesized to balance dilution. In the main text, we argued that the principal effect of dilution is to introduce an effective degradation rate set by the cell doubling time. Here, we show that this is indeed the case: We study a model in which growth, cell division, and binomial partitioning of the proteins upon cell division are modeled explicitly (15) and show that its qualitative behavior is similar to the model of the main text, in which the volume is held constant and protein degradation occurs at a rate that is constant in time.

The model we consider here is the *PPC-TTC* model presented in the main text, but with the degradation reaction, **9**, replaced by a scheme in which the bacterial volume  $V$  grows exponentially as

$$V(t) = V_0 e^{\frac{t \ln 2}{T_d}}, \quad [\text{S33}]$$

where  $T_d$  denotes the doubling time after which the volume reaches twice its minimum  $V_0$  and cell division is triggered. Division includes dividing the volume by two, partitioning the proteins binomially (15), and deleting events on the queue of the delay associated with the KaiC production reaction with a probability of 0.5 for each daughter cell. To compare the results of this model with those from the main text, we take  $T_d = \ln 2/\mu$ , where  $\mu$  is the protein degradation rate of the model in the main text; if proteins were to decay only by dilution in a cell with a doubling time  $T_d$ , then  $\mu$  would be the effective protein degradation rate; if proteins are also degraded actively, then  $\mu = \ln 2/T_d$  is a lower bound on the actual degradation rate.

Fig. S5G and H show time traces of the total KaiC concentration and the KaiC phosphorylation level for this refined model. It is seen that the oscillations of the total KaiC concentration are more noisy than those in the model in which the Kai proteins are degraded with rates that are constant in time (Fig. S1C). Clearly, binomial partitioning is a major source of noise, with the random removal of items from the queue associated with the KaiC synthesis reaction being the largest source of noise. Nonetheless, the oscillations of the KaiC phosphorylation level are much less affected, with the correlation number of cycles being  $n_{1/2} = 88$ . Indeed, while this model combining a TTC with a PPC is fairly robust, an oscillator with exponential volume growth and binomial partitioning built upon a TTC alone, is not stable. This supports our statement in the main text that a PPC can strongly enhance the robustness of a TTC. In future work, we will systematically study the effect of bursts in gene expression and binomial partitioning.

**S5. An Alternative PPC-in Vitro Model: The Rust Model.** In the main text, we argue that the synergy between a transcription-translation cycle and a protein modification cycle is a generic feature of clocks that exploit both cycles. To support this claim, we have studied a model in which our model of the PPC is replaced by that of Rust et al. (8). This model describes a phosphorylation cycle at the level of KaiC monomers, rather than KaiC hexamers as in our model. In the Rust model, each KaiC monomer cycles between an unphosphorylated state “U,” a singly phosphorylated state “T,” where KaiC is phosphorylated at threonine 432, a doubly phosphorylated state “ST,” where KaiC is phosphorylated at threonine 432 and serine 431, and a singly phosphorylated state “S,” where KaiC is phosphorylated at serine 431 (8, 16). This cycle is described by the reactions



with reaction rates given by equation 5 of the supplementary material of Rust et al. (8). These rates depend on the concentration of free KaiA, which is sequestered by KaiC in the S state. We model KaiA sequestration explicitly:



We picture sequestration to be fast and we picked a forward rate of  $1.72 \cdot 10^{12} \text{ 1/Mh}$  and a backward rate of  $\text{h}^{-1}$  for both equations above. Dephosphorylation of KaiC in the S state might occur even when KaiA is bound, in which case the KaiA protein is released from the complex. We define the output signal as

$$p(t) = \frac{[T] + [ST] + [S] + [AS] + [A_2S]}{[U] + [T] + [ST] + [S] + [AS] + [A_2S]}, \quad [\text{S36}]$$

which resembles the phosphorylation ratio in the case where we cannot distinguish between singly and doubly phosphorylated



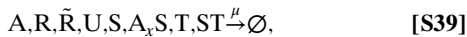
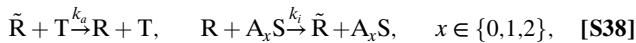
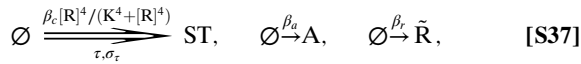
KaiC. The denominator in the above expression is also the total KaiC monomer concentration. We use the same concentrations as Rust et al.,  $[KaiA] = 1.3 \mu\text{M}$  (active KaiA monomers) and  $[KaiC] = 3.4 \mu\text{M}$  (KaiC monomers), and simulate this model using the Gillespie algorithm (2).

When we simulate this model for a volume  $V = 1 \mu\text{m}^3$ , we find a period of  $L = 21.4 \text{ h}$  and a decay constant for the autocorrelation function of  $\tau_d = 128 \text{ h}$ . The corresponding correlation number of cycles is  $n_{1/2} = 30$ , which is lower than that observed experimentally,  $n_{1/2} = 166 \pm 100$  (5), and lower than that of the PPC developed by us (1), for which  $n_{1/2} \approx 200$  (see Fig. 2 of the main text). This is because the model of Rust et al. features a phosphorylation cycle at the level of KaiC monomers rather than KaiC hexamers as in our model. The concomitant reduction in the total number of phosphorylation steps in the cycle reduces the robustness in the model of Rust et al. (8).

**55.1. An alternative PPC-in vivo model: The Rust model with constant protein synthesis and degradation.** To study the behavior of the model of Rust et al. (8) under conditions in which cells grow and divide, we have to include protein degradation and make up for this by protein synthesis. As in the main text, when we vary the protein degradation rates, we adjust the protein synthesis rates such that the average protein concentrations are unchanged and similar to those used in the in vitro experiments (3, 4).

Fig. S6A shows the results for this model. They are qualitatively the same as those of Fig. 3 of the main text: The robustness decreases with decreasing volume and increasing degradation rate. Hence, not only in our model but also in that of Rust et al. (8), protein degradation can cause the oscillations to disappear. This supports our claim that a protein modification oscillator cannot function on its own when the cell's growth rate is high enough.

**55.2. An alternative PPC-TTC model: The Rust model with a TTC.** We will now show that a TTC can resurrect the PPC of Rust et al. (8). We model the TTC as



where the first line describes the production of proteins to counteract their degradation and the second line summarizes the RpaA signaling pathway, where KaiC that is phosphorylated at the T site activates RpaA and KaiC that is phosphorylated at the S site represses RpaA activation. The parameters in this model are  $\beta_c = 1.16 \mu\text{M}/\text{h}$ ,  $K = 0.058 \mu\text{M}$ ,  $\beta_a = 0.13 \mu\text{M}/\text{h}$ ,  $\beta_r = 0.058 \mu\text{M}/\text{h}$ ,  $k_a = k_i = 1.71 \cdot 10^9 \text{ 1/Mh}$ ,  $\mu = 0.1 \text{ h}^{-1}$ , and the delay is  $\tau = (3 \pm 0.3) \text{ h}$ . Fig. S6B shows the results of this model at a volume  $V = 1 \mu\text{m}^3$ . Analyzing the autocorrelation function, we find a period  $L = 22.5 \text{ h}$  and a correlation decay time of  $\tau = 1.832 \text{ h}$  leading to a correlation number of cycles of  $n_{1/2} = 402$ . Clearly, a TTC can also resurrect the PPC of Rust et al. (8), supporting our claim that the qualitative results of the main text should apply to any biological system that exploits both a protein modification cycle and a protein synthesis cycle to generate circadian rhythms.

**56. PPC-TTC Model: Period as a Function of Cell Volume and Protein Degradation Rate.** Fig. S7 shows the period of the oscillation of the KaiC phosphorylation level in the full PPC-TTC model of the main text (1–9) as a function of the cell volume and the pro-

tein degradation rate. As before, the protein synthesis rates are adjusted such that the average protein concentrations are constant and similar to those used in the in vitro experiments (3, 4). It is seen that the dependence of the oscillation period on the cell volume and protein degradation rate is rather weak. This is because the rhythm of the clock is dictated by the PPC, which is insensitive to the absolute rates of protein synthesis and decay. We note here that the period of the oscillation, as well as its amplitude, would change if the *ratio* of the concentrations of the Kai proteins were changed. Although the dependence of both the amplitude and the period of the in vitro PPC on the ratio of the concentrations of the Kai proteins has been characterized in detail (3, 4), the dependence of the in vivo oscillator on their ratio has not been studied experimentally.

**57. Measuring the Robustness.** In this section, we discuss how we calculate the correlation number of cycles  $n_{1/2}$  for our various models. We begin with some theoretical background: Consider a phase variable  $\varphi(t)$  that increases with an average frequency  $\omega$  and is also subject to noise. Its time evolution can be written as

$$\frac{d\varphi(t)}{dt} = \omega + \xi(t) \quad \text{with} \quad \langle \xi(t)\xi(t') \rangle = \sigma^2 \delta(t-t'). \quad [\text{S40}]$$

Here  $\xi(t)$  is Gaussian white noise of strength  $\sigma^2$ , and  $\langle \cdot \rangle$  indicates averaging over different realizations of the noise. Integrating the equation with the initial condition  $\varphi(0) = 0$  yields

$$\varphi(t) = \omega t + \mathcal{W}(t), \quad [\text{S41}]$$

where  $\mathcal{W}(t)$  is a Gaussian random variable with mean zero and variance

$$\langle (\varphi(t) - \omega t)^2 \rangle = \sigma^2 t. \quad [\text{S42}]$$

From this, we can construct an oscillating signal

$$x(t) = x_0 + a \cdot \sin \varphi(t) \quad [\text{S43}]$$

with mean  $x_0$  and amplitude  $a$ . The autocorrelation function of **44** is then

$$C(t') = \frac{\langle \delta x(t) \delta x(t+t') \rangle}{\langle \delta x(t)^2 \rangle} = e^{-\frac{1}{4}\sigma^2|t'|} \cdot \cos(\omega t'), \quad [\text{S44}]$$

where  $\delta x(t) \equiv x(t) - x_0$  is the deviation of the signal from its average value  $x_0$ . We thus expect that the correlation function is a sinusoid modulated by a single exponential decay.

**57.1. Incorporating amplitude noise.** Because the phase is the only “soft” direction of the dynamical system, one generically expects any noisy oscillator at long times to act similarly to the simple model of a phase oscillator just described. Nonetheless, a more realistic description would also include a fluctuating amplitude. We incorporate this behavior phenomenologically by including a time dependence in the amplitude:

$$a \rightarrow a(t) = a_0 + \xi_{(a)}(t) \Rightarrow x(t) = x_0 + [a_0 + \xi_{(a)}(t)] \cdot \sin[\omega t + \mathcal{W}(t)], \quad [\text{S45}]$$

where  $\xi_{(a)}(t)$  denotes a Gaussian white noise process of strength  $\sigma_a^2$  and therefore neglects correlations in the amplitude fluctuations. We can again calculate the correlation function analytically. By definition, we have  $C(0) = 1$  for  $t = 0$ , but because  $a(t)$  now contains a white noise term,  $C(t)$  jumps discontinuously to a smaller value for any  $t > 0$ . One finds

$$C(t') = \frac{\langle \delta x(t) \delta x(t+t') \rangle}{\langle \delta x(t)^2 \rangle} = \frac{a_0^2}{\underbrace{a_0^2 + \sigma_a^2}_{=\nu}} e^{-\frac{1}{2}\sigma^2|t'|} \cdot \cos(\omega t'), \quad t' > 0.$$

[S46]

Considering the more natural case of a finite correlation time in the amplitude noise, the picture will only change slightly: Instead of jumping from 1 to  $\nu$  at  $t' = 0$ , the envelope will undergo a smooth transition involving two time scales: a short time scale of the order of the correlation time of the amplitude fluctuations and a much longer time scale associated with the phase diffusion. In practice, we found that including amplitude fluctuations did not significantly change our estimate for  $n_{1/2}$ .

**57.2. Computing the correlation number of cycles.** To calculate the correlation number of cycles  $n_{1/2}$ , we begin by using our simulation results to estimate the correlation function  $C(t)$ . After an initial equilibration phase of 500 h, we do simulations for 50,000 h. From these, we extract  $N = 500,000$  values  $x_i$  for the time trace  $x(t)$  at equidistant points in time, which we can then use to calculate the correlation function at times separated by an interval  $\Delta t = 0.1$  h:

$$x_i = x(t_0 + i \cdot \Delta t), \quad C(i \cdot \Delta t) = \frac{1}{(N-i) \cdot \langle \delta x^2 \rangle} \sum_{j=0}^{N-i} \delta x_j \delta x_{j+i}.$$

[S47]

Here  $x(t)$  is either the phosphorylation level  $p(t)$  or the total concentration of KaiC hexamers.  $p(t)$  is used for all cases except for models where there is only a TTC and a phosphorylation level cannot be defined.

Once  $C(t)$  has been computed, it can be fitted to the form S46 to determine the free parameters  $\nu$ ,  $\sigma^2$ , and  $\omega$ . In practice we perform the fit using `gnuplot`, which in turn implements a Marquardt–Levenberg algorithm.

Finally, it remains to translate the fitted parameter values into an estimate of  $n_{1/2}$ . Eguchi et al. define  $n_{1/2}$  as the number of cycles after which the standard deviation of the phase is  $\pi$  (7). Thus, we have

$$\sqrt{\langle [\varphi(L \cdot n_{1/2}) - \omega t]^2 \rangle} = \pi \Rightarrow n_{1/2} = \frac{\pi^2}{L\sigma^2}, \quad [\text{S48}]$$

where  $L = 2\pi/\omega$  denotes the period and we have used Eq. S42 to solve the left equation for  $n_{1/2}$ . The value of  $n_{1/2}$  is then obtained by substituting the fitted values for  $\sigma^2$  and  $\omega$ . Using this method we can reliably measure  $n_{1/2}$  from 1 to 1,000. The upper bound is given by the fact that we compute the correlation function  $C(t)$  only up to  $t = 3,000$  h and therefore correlation functions that decay on much longer time scales are difficult to detect.

Concerning the error bar on the computed  $n_{1/2}$ , it should be noted that there are two distinct sources of error: one due to statistical fluctuations, and one due to systematic errors, e.g., that the correlation function cannot be fitted to Eq. S46. To estimate the former, for certain parameter values we repeated the procedure described above 32 times, i.e., we performed 32 independent simulations and computed the mean and the standard deviation of the set of 32 independently estimated values for  $n_{1/2}$ . For  $V = 1 \mu\text{m}^3$  and  $\mu = 0.025 \text{ h}^{-1}$ , this gave  $n_{1/2} = 168 \pm 31$  (mean  $\pm$  SD) for the combined PPC-TTC model. To address the second type of error, we also computed  $n_{1/2}$  using two different methods. One is the method of Eguchi et al., which is based on examining the times at which the oscillation reaches its maximum in each cycle and thus does not assume any particular form like Eq. S43 for the oscillating signal (7). The other method involves computing the

width of the dominant peak in the power spectrum of the time traces. The three methods gave similar error bars and values for  $n_{1/2}$  that agree within the error bar. Although all methods gave the same result, we found the method based on the correlation function (Eq. S46) more robust for noisy oscillations at low cell volumes.

**Appendix: Crossing-Time Distribution in TTC-Only and PMS-TTC Models.** We imagine that at  $t = 0$  we have  $N$  repressor molecules, which can only decay; they can either decay via degradation only, as in the TTC-only model, or decay via a combination of degradation and a sequence of modification steps, as in the PMS-TTC model. The aim is now to compute the distribution of times the system crosses the repression threshold at a later time  $t$ . We imagine that the repression threshold is crossed when the number of molecules  $M(t)$  at time  $t$  drops below  $M_c$ , thus when  $M$  goes from  $M_c$  to  $M_c - 1$ . This yields the following expression for the (normalized) distribution of crossing times:

$$P_c(t) = M_c q(t) \frac{N!}{(N - M_c)! M_c!} S(t)^{M_c - 1} (1 - S(t))^{N - M_c}, \quad [\text{S49}]$$

where  $S(t)$  is the survival probability, which is the probability that a molecule has not decayed at later time  $t$ , and  $q(t) = -\partial S(t)/\partial t$  is the probability per unit amount of time that a molecule, given that it is active at  $t = 0$ , decays at a later time  $t$ .

The task is now to compute  $S(t)$ . In the TTC-only model the molecules can decay only via degradation, and the survival probability is simply  $S(t) = e^{-\mu t}$ , where  $\mu$  is the degradation rate. For the PMS-TTC model, we assume that the molecules start in the repressing  $\tilde{C}_6$  state. They can then go through a sequence of irreversible protein modification steps  $\tilde{C}_6 \rightarrow \tilde{C}_5 \rightarrow \dots \rightarrow \tilde{C}_1 \rightarrow \tilde{C}_0$ , and then switch to the nonrepressing  $C_0$  state; moreover, in each state they can also decay via degradation. Each modification reaction occurs at a rate  $\lambda = k_{\text{dps}}$ , degradation proceeds with a rate  $\mu$ , and the switch from  $\tilde{C}_0$  to  $C_0$  occurs with rate  $b_0$ . A molecule is still active as a repressor when it is in one of the  $\tilde{C}_6, \tilde{C}_5, \dots, \tilde{C}_1, \tilde{C}_0$  states, meaning that the survival probability is given by

$$S(t) = \sum_{i=0}^6 P_i(t), \quad [\text{S50}]$$

where  $P_i(t)$  is the probability that a molecule is in state  $\tilde{C}_i$  at time  $t$ . For  $i = 1, 2, \dots, 5, 6$ , it is given by

$$P_i(t) = \frac{(\lambda t)^{6-i}}{(6-i)!} e^{-(\lambda+\mu)t}. \quad [\text{S51}]$$

Indeed, this equation holds for all the repressing states except the last one, because in this state  $\tilde{C}_0$  the molecule can become nonrepressing not only via degradation, but also by switching to the nonrepressing state  $C_0$  state. The probability of being in the  $\tilde{C}_0$  at time  $t$  is

$$P_0(t) = \lambda \int_0^t dt' P_1(t') e^{-(b_0+\mu)(t-t')}, \quad [\text{S52}]$$

$$= \frac{\lambda^6}{5!} e^{-(\mu+b_0)t} \int_0^t dt' t'^5 e^{-(\lambda-b_0)t'}, \quad [\text{S53}]$$

which can be solved analytically by iteratively integrating by parts. Clearly, if  $b_0 = \lambda$  the above expression reduces to Eq. S51 for  $i = 0$ . It is also clear that if  $b_0 \rightarrow \infty$ ,  $P_0(t)$  becomes zero and  $S(t) = \sum_{i=1}^6 P_i(t)$ . Finally, if  $\lambda = 0$ , this model reduces to the TTC-only model.



- van Zon JS, Lubensky DK, Altena PRH, ten Wolde PR (2007) An allosteric model of circadian KaiC phosphorylation. *Proc Natl Acad Sci USA* 104:7420–7425.
- Gillespie DT (1977) Exact stochastic simulation of coupled chemical reactions. *J Phys Chem* 81:2340–2361.
- Kageyama H, et al. (2006) Cyanobacterial circadian pacemaker: Kai protein complex dynamics in the KaiC phosphorylation cycle in vitro. *Mol Cell* 23:161–171.
- Nakajima M, Ito H, Kondo T (2010) In vitro regulation of circadian phosphorylation rhythm of cyanobacterial clock protein KaiC by KaiA and KaiB. *FEBS Lett* 584(5):898–902.
- Mihalcescu I, Hsing W, Leibler S (2004) Resilient circadian oscillator revealed in individual cyanobacteria. *Nature* 430:81–85.
- Kitayama Y, Iwasaki H, Nishiwaki T, Kondo T (2003) KaiB functions as an attenuator of KaiC phosphorylation in the cyanobacterial circadian clock system. *EMBO J* 22:2127–2134.
- Eguchi K, Yoda M, Terada TP, Sasai M (2008) Mechanism of robust circadian oscillation of KaiC phosphorylation in vitro. *Biophys J* 95:1773–1784.
- Rust MJ, Markson JS, Lane WS, Fisher DS, O'Shea EK (2007) Ordered phosphorylation governs oscillation of a three-protein circadian clock. *Science* 318:809–812.
- Imai K, Nishiwaki T, Kondo T, Iwasaki H (2004) Circadian rhythms in the synthesis and degradation of a master clock protein KaiC in cyanobacteria. *J Biol Chem* 279:36534–36539.
- Ermentrout B (2002) *Simulating, Analyzing, and Animating Dynamical Systems: A Guide to Xppaut for Researchers and Students* (SIAM, Philadelphia).
- Ozbudak EM, Thattai M, Kurtser I, Grossman AD, van Oudenaarden A (2002) Regulation of noise in the expression of a single gene. *Nat Gen* 31:69–73.
- Golding I, Paulsson J, Zawilski SM, Cox EC (2005) Real-time kinetics of gene activity in individual bacteria. *Cell* 123:1025–1030.
- van Zon JS, Morelli M, Tănase-Nicola, Ten Wolde PR (2006) Diffusion of transcription factors can drastically enhance the noise in gene expression. *Biophys J* 91:4350–4367.
- Gonze D, Halloy J, Gaspard P (2002) Biochemical clocks and molecular noise: Theoretical study of robustness factors. *J Chem Phys* 116:10997–11010.
- Swain PS, Elowitz MB, Siggia ED (2002) Intrinsic and extrinsic contributions to stochasticity in gene expression. *Proc Natl Acad Sci USA* 99:12795–12800.
- Nishiwaki T, et al. (2007) A sequential program of dual phosphorylation of KaiC as a basis for circadian rhythm in cyanobacteria. *EMBO J* 26:4029–4037.
- Kitayama Y, Nishiwaki T, Terauchi K, Kondo T (2008) Dual KaiC-based oscillations constitute the circadian system of cyanobacteria. *Genes Dev* 22:1513–1521.

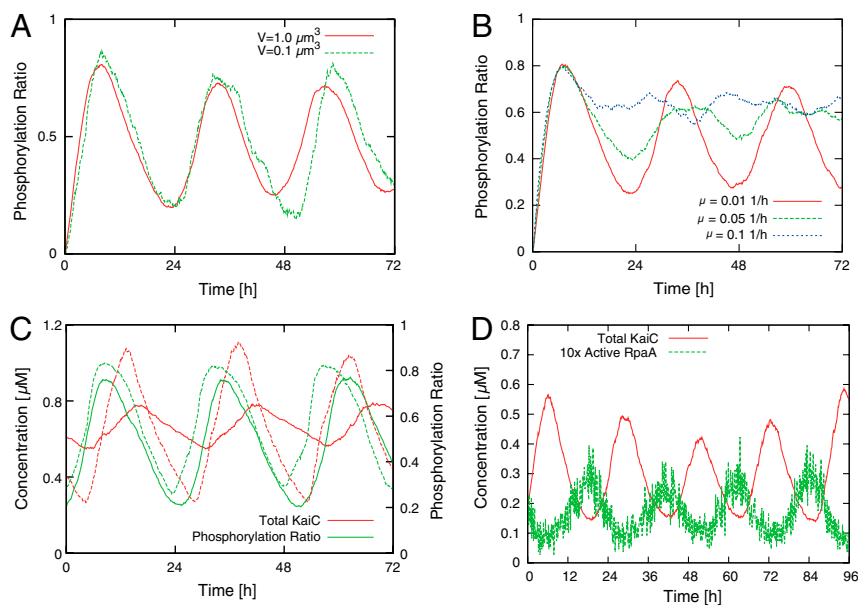


**Fig. S1.** Time traces of the different models studied in the main text. (A) *PPC-in vitro* model, a PPC model in which the concentration of each Kai protein is constant. Time traces of the phosphorylation level  $p(t)$ , defined as the fraction of monomers that is phosphorylated, for two different volumes. The correlation number of cycles,  $n_{1/2}$ , as a function of volume is shown in Fig. 2 of the main text. (B) *PPC-in vivo* model, a PPC model in which the Kai proteins are continually being produced and degraded. Time traces of the phosphorylation level  $p(t)$  for three different degradation rates  $\mu$ . The correlation number of cycles,  $n_{1/2}$ , as a function of volume and the degradation rate is shown in Fig. 3 of the main text. (C) *PPC-TTC* model, which combines a PPC with a TTC. Time traces of the phosphorylation level  $p(t)$  and total KaiC concentration  $[C]_T(t)$  for  $V = 1 \mu\text{m}^3$  and  $\mu = 0.03 \text{ h}^{-1}$  (solid lines) and  $\mu = 0.1 \text{ h}^{-1}$  (dashed lines). The correlation number of cycles,  $n_{1/2}$ , as a function of volume and the degradation rate is shown in Fig. 4 of the main text. Time traces of RpaA are shown in Fig. S5C. (D) *TTC-only* model. Time traces of the concentrations of active RpaA and KaiC ( $V = 1 \mu\text{m}^3$  and  $\mu = 0.15 \text{ h}^{-1}$ ). The (average) concentrations of KaiA, KaiB, and KaiC are those used in the in vitro experiments (3, 4):  $[A]_T = 0.58 \mu\text{M}$ ;  $[B]_T = 1.75 \mu\text{M}$ ;  $[C]_T = 0.58 \mu\text{M}$ . For other parameter values, see Table S1.









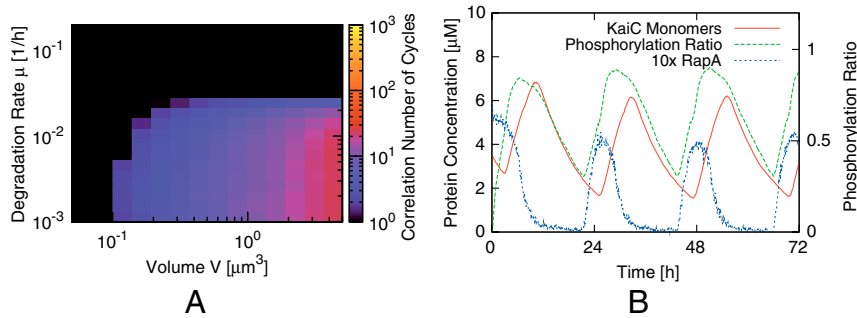


**Fig. 56.** Robustness of a *PPC-in vivo* (A) and a *PPC-TTC* model (B), where the PPC is based on the model of Rust et al. (8). (A) Contour plot of  $n_{1/2}$  of the PPC model of Rust et al. but with production and degradation of Kai proteins with rates that are constant in time, as a function of the degradation rate  $\mu$  and the volume  $V$ . (B) Time trace of the Rust model (8) extended to include a TTC for  $V = 1 \mu\text{m}^3$ . Both the total concentration of KaiC and the phosphorylation level of KaiC show stable oscillations. The messenger protein RpaA concentration is shown tenfold and crosses the threshold of  $K = 0.174 \mu\text{M}$  ( $\approx 100$  molecules) reliably.

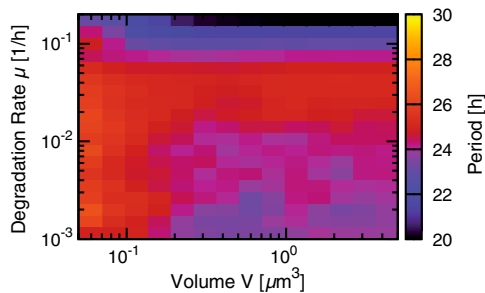


**Fig. 57.** Period of the oscillation in the KaiC phosphorylation level in the full *PPC-TTC* model of the main text as a function of cell volume and protein degradation rate. When the degradation rate is varied, the protein synthesis rates are adjusted such that the average protein concentrations are constant and similar to those used in the *in vitro* experiments (3, 4). The period is essentially independent of the volume and exhibits only a weak dependence on the degradation rate  $\mu$ .

**Table S1. The parameters used for the full models of the main text and the minimal models of section S2**

| Constant                                      | Value  | Constant                 | Value                                  |
|---|--|--------------------------|--|
| <b>PPC (1-5 and S1-S5):</b>                   |  |                          |  |
| $k_{ps}, \bar{k}_{ps}$                        | 0.025 1/h  | $k_{dps}, \bar{k}_{dps}$ | 100 1/h                                |
| $k_{pf}$                                      | 1.0 1/h  | $b_i$                    | 100 1/h                                |
| $f_i$   | $\{10^{-6}, 10^{-5}, 10^{-4}, 10^{-3}, 10^{-2}, 10^{-1}, 10\}$ 1/h                     | $k_i^{Ab}$               | $\{1, 3, 9, 27, 81, 243, 729\}$ 1/h    |
| $k_i^{Af}$                                    | $1.72 \cdot 10^{10}$ 1/M·h   | $\bar{k}_i^{Bb}$         | $\{10, 1, 1, 1, 1, 1\}$ 1/h            |
| $\bar{k}_i^{Bf}$                              | $1.72 \cdot 10^9 \times \{0.001, 0.1, 1, 1, 1, 1\}$ 1/M·h                              |                          |  |
| $k_i^{Af}$                                    | $1.72 \cdot 10^9 \times \{10^{-2}, 10^3, 10^3, 10^3, 10^2, 10^{-3}, 10^{-4}\}$ 1/M·h   |                          |  |
| $\bar{k}_i^{Ab}$                              | $\{10, 1, 1, 1, 1, 1, 10\}$ 1/h  |                          |  |
| <b>Deterministic PPC (Eqs. S8-S11):</b>       |  |                          |  |
| $\bar{k}_i^{Bf}$                              | $2.97 \cdot 10^{18} \times \{0.01, 1, 1, 1, 1, 1\}$ 1/M <sup>2</sup> ·h                | $\bar{k}_i^{Bb}$         | $100 \times \{10, 1, 1, 1, 1, 1\}$ 1/h |
| $K_i$   | $3.37 \cdot 10^{-25} \times \{\infty, 100, 1, 1, 100, \infty, \infty\}$ M <sup>2</sup> |                          |  |
| <b>RpaA activation (6 and S12):</b>           |  |                          |  |
| $k_a$   | $8.6 \cdot 10^9$ 1/M·h   | $k_i$                    | $4.3 \cdot 10^9$ 1/M·h                 |
| <b>TTC (7-9 and S13 and S14):</b>             |  |                          |  |
| $K$   | 0.058 $\mu$ M  | $\beta_r$                | $\mu^{-1} \times 0.29$ $\mu$ M         |
| $\beta_a$                                     | $\mu^{-1} \times 0.58$ $\mu$ M   | $\sigma_\tau$            | 0.5 h                                  |
| $\tau$  | 5 h  |                          |  |
| <b>RpaA activation TTC-only (11 and S16):</b> |  |                          |  |
| $k_a^t$                                       | 1 1/M·h  | $k_i^t$                  | 100 1/M·h                              |
| <b>Minimal PPC (S17-S20):</b>                 |  |                          |  |
| $k_{dps}, \bar{k}_{dps}$                      | 0.375 1/h  | $k_{pf}$                 | 1.0 1/h                                |
| $f_6$   | 100 1/h  | $b_0$                    | 90 1/h                                 |
| $k_i^{Af}$                                    | $1.72 \cdot 10^{10}$ 1/M·h   | $k_i^{Ab}$               | $\{1, 3, 9, 27, 81, 243, 729\}$ 1/h    |
| $\bar{k}_i^{Af}$                              | $1.72 \cdot 10^9 \times \{10^{-2}, 10^3, 10^3, 10^3, 10^2, 10^{-3}, 10^{-4}\}$ 1/M·h   |                          |  |
| $\bar{k}_i^{Ab}$                              | $\{10^6, 10^3, 10^{-2}, 10^{-3}, 10^{-3}, 10^{-3}, 10^3\}$ 1/h                         |                          |  |
| <b>Minimal TTC (S21-S23):</b>                 |  |                          |  |
| $K$   | 0.29 $\mu$ M   | $\beta_a$                | $\mu^{-1} \times 0.58$ $\mu$ M         |
| $\tau$  | 8 h  | $\sigma_\tau$            | 0.8 h                                  |

The degradation rate  $\mu$  is a free parameter that we vary to explore different growth conditions. The numbers between the curly brackets correspond to the different KaiC phosphorylation states  $i$  in ascending order; values of  $\infty$  for  $K_i$  indicate that a particular binding reaction is not allowed. The production rate  $\beta_c$  is determined from an optimization for the mean protein concentration  $\langle [C] \rangle = 0.58$   $\mu$ M.

**Table S2. Models with different output pathways from the PPC to the TTC**

| Model | Activator                         | Repressor                                     | Threshold $K$ | $n_{1/2}$ |
|-------|-----------------------------------|---|---------------|-----------|
| a     | $AC_2, AC_3, AC_4, AC_5$          | $A_y B_x \bar{C}_2, \dots, A_y B_x \bar{C}_5$ | 0.058 $\mu$ M | 195       |
| b     | $AC_3, AC_4$                      | $A_y B_x \bar{C}_2, \dots, A_y B_x \bar{C}_6$ | 0.058 $\mu$ M | 118       |
| c     | $AC_3, AC_4$                      | $A_y B_x \bar{C}_3, \dots, A_y B_x \bar{C}_4$ | 0.058 $\mu$ M | 180       |
| d     | $C_3, AC_3, C_4, AC_4$            | $A_y B_x \bar{C}_3, \dots, A_y B_x \bar{C}_4$ | 0.029 $\mu$ M | 39        |
| e     | $C_x, AC_x, x \in \{2, 3, 4, 5\}$ | $A_y B_x \bar{C}_3, \dots, A_y B_x \bar{C}_4$ | 0.029 $\mu$ M | 48        |

These models differ in the choice of phosphoforms that activate and repress RpaA, respectively. The maximal production rate  $\beta_c$  has been modified such that the average concentration of KaiC is 0.58  $\mu$ M, as used in the in vitro experiments (3, 4). In each case,  $n_{1/2}$  is given for a volume  $V = 1$   $\mu$ m<sup>3</sup> and a decay rate  $\mu = 0.03$  h<sup>-1</sup>. Model a is the PPC-TTC model from the main text. To make the simulations tractable, we neglected repression of RpaA activation by KaiC phosphoforms that occur in negligible concentrations; consequently, the full list of phosphoforms that has the potential to repress RpaA is  $\{B_2 \bar{C}_6, B_2 \bar{C}_5, AB_2 \bar{C}_5, A_2 B_2 \bar{C}_5, B_2 \bar{C}_4, AB_2 \bar{C}_4, A_2 B_2 \bar{C}_4, B_2 \bar{C}_3, AB_2 \bar{C}_3, A_2 B_2 \bar{C}_3, B_2 \bar{C}_2, AB_2 \bar{C}_2, A_2 B_2 \bar{C}_2\}$ . Other parameters are given in Table S1